

Electronic Structure of Novel Superconductor $\text{Ca}_4\text{Al}_2\text{O}_6\text{Fe}_2\text{As}_2$

Takashi Miyake,^{1,4,5} Taichi Kosugi,^{1,3} Shoji Ishibashi^{1,4} and Kiyoyuki Terakura²

¹*Nanosystem Research Institute (NRI) "RICS", AIST, Umezono, Tsukuba 305-8568, Japan*

²*Research Center for Integrated Science (RCIS), JAIST Asahidai, Nomi, Ishikawa 923-1292, Japan*

³*Department of Physics, University of Tokyo, Bunkyo, Tokyo 113-0033, Japan*

⁴*JST, Transformative Research-Project on Iron Pnictides (TRIP), Sanbancho, Chiyoda, Tokyo 102-0075, Japan*

⁵*JST, Core Research for Evolutional Science and Technology (CREST), Honcho, Kawaguchi, Saitama 332-0012, Japan*

(Received November 26, 2018)

We have performed the first-principles electronic structure calculation for the novel superconductor $\text{Ca}_4\text{Al}_2\text{O}_6\text{Fe}_2\text{As}_2$ which has the smallest a lattice parameter and the largest As height from the Fe plane among the Fe-As superconductors. We find that one of the hole-like Fermi surfaces is missing around the Γ point compared to the case of LaFeAsO . Analysis using the maximally-localized-Wannier-function technique indicates that the xy orbital becomes more localized as the As-Fe-As angle decreases. This induces rearrangement of bands, which results in the change of the Fermi-surface topology of $\text{Ca}_4\text{Al}_2\text{O}_6\text{Fe}_2\text{As}_2$ from that of LaFeAsO . The strength of electron correlation is also evaluated using the constraint RPA method, and it turns out that $\text{Ca}_4\text{Al}_2\text{O}_6\text{Fe}_2\text{As}_2$ is more correlated than LaFeAsO .

KEYWORDS: $\text{Ca}_4\text{Al}_2\text{O}_6\text{Fe}_2\text{As}_2$, electronic structure, first-principles calculation, maximally-localized Wannier function

The discovery of the new iron-pnictide superconductor $\text{LaO}_{1-x}\text{F}_x\text{FeAs}$ ¹⁾ stimulated extensive work to clarify the basic features of material properties, particularly the origin and character of superconductivity and also to search for new superconductors. In fact, a variety of related superconductors have been synthesized: they have the topologically identical iron (Fe)-pnictogen (Pn) layer structure combined with various block layers.²⁻⁴⁾ Among them, a family of materials which have block layers of the perovskite structure are unique in the sense that the distance between the neighboring Fe-Pn layers can be systematically controlled by changing the thickness of the block layer.⁴⁾ The rich variation of the materials with the perovskite structure is also attractive. Quite recently, Ogino *et al.* synthesized $(\text{Ca}_{n+2}(\text{Al},\text{Ti})_n\text{O}_{3n-y})(\text{Fe}_2\text{As}_2)$ ($n=2,3,4$) and observed the start of resistivity drop at about 39 K for $n=4$.⁵⁾ For the synthesis of these materials at ambient pressure, the presence of Ti turns out to be essential not to produce strong internal strain. However, subsequent to this work, Shirage *et al.* have successfully synthesized $\text{Ca}_4\text{Al}_2\text{O}_{6-y}\text{Fe}_2\text{Pn}_2$ with Pn=P and As without Ti using a high-pressure synthesis technique.⁶⁾ The superconducting transition temperatures are 17.1 K for P and 28.3 K for As. These materials are characterized by the smallest a -lattice parameters and the largest pnictogen heights from the Fe plane among the iron-pnictide superconductors. It is pointed out that these quantities are crucial in determining the transition temperature.⁷⁻¹⁰⁾

In the present work, we have performed DFT calculations for $(\text{Ca}_4\text{Al}_2\text{O}_{6-y})(\text{Fe}_2\text{As}_2)$ in order to analyze the effects of the above unique structural features on the electronic structures paying particular attention to the energy range near the Fermi level. The absence of Ti in this material makes our analysis simpler because

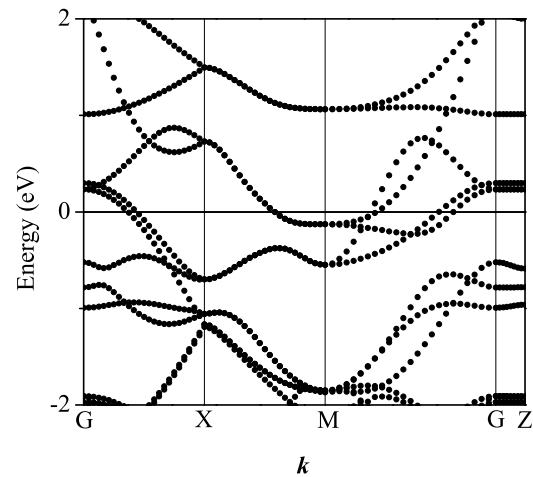


Fig. 1. Non-magnetic electronic band structure for $\text{Ca}_4\text{Al}_2\text{O}_6\text{Fe}_2\text{As}_2$. The Fermi level corresponds to the energy zero.

d states near the Fermi level comes only from Fe. We used a computational code QMAS¹¹⁾ based on the projector augmented-wave method,¹²⁾ which has been applied to the study of the ground state properties of LaFeAsO ^{13,14)} and SrFe_2As_2 .¹⁵⁾ The generalized gradient approximation (GGA)¹⁶⁾ was adopted for the electronic exchange correlation energy. The electronic band structure in the vicinity of the Fermi level is analyzed in detail using the maximally-localized Wannier function technique^{17,18)} combined with the full-potential linear muffin-tin orbital (FP-LMTO) method¹⁹⁾ in the local density approximation (LDA).²⁰⁾

Figures 1 and 2 represent the non-magnetic electronic band structure and density of states for the experimental structure of $\text{Ca}_4\text{Al}_2\text{O}_6\text{Fe}_2\text{As}_2$ ⁶⁾ in GGA obtained by QMAS. We found that LDA (using the FP-LMTO code) gives almost the same result. As with other iron-pnictide

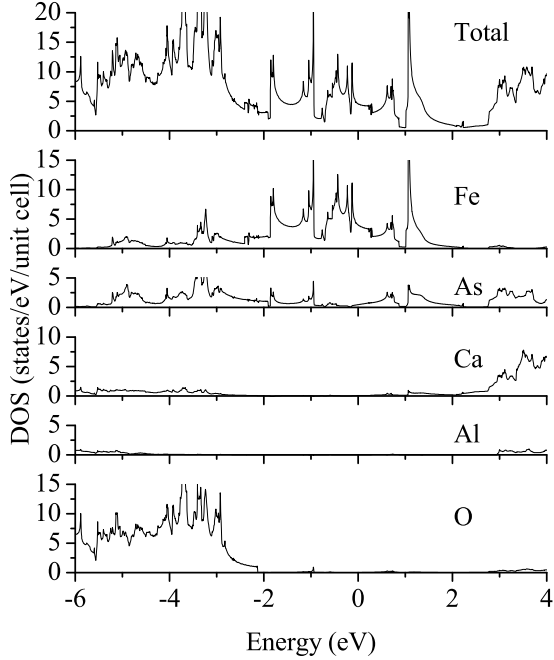


Fig. 2. Electronic density of states (DOS) and partial DOS's for $\text{Ca}_4\text{Al}_2\text{O}_6\text{Fe}_2\text{As}_2$. The Fermi level corresponds to the energy zero.

superconductors, electronic states near the Fermi level derive predominantly from the Fe 3d orbitals though there is significant contribution of As 4p states. In Fig. 3 (a), the Fermi surfaces are shown for the undoped case and the doped cases with ± 0.1 electrons/Fe obtained by the rigid band approximation. There are two electron-like surfaces centered at the M point. This is a common feature among the iron-pnictide superconductors. On the other hand, there are two hole-like surfaces around the Γ point. This is in sharp contrast with other iron-pnictide superconductors, where three hole-like surfaces are formed. We will discuss this point later. To examine the nesting property, a bare generalized susceptibility is calculated and plotted in Fig. 3 (b). There is a nesting feature from Γ to M. While the change is small with hole doping, it is reduced significantly with electron doping, suggesting that the magnetic instability is suppressed under electron doping. In the actual samples, oxygen content $6 - y = 5.6$ to 5.8 will produce doping of 0.2 to 0.4 electrons/Fe.

In order to analyze the electronic structure in more detail, we projected out energy bands near the Fermi energy and constructed ten maximally localized Wannier functions. The Wannier functions are characterized by the shapes closely related to the Fe 3d orbitals though there are significant amplitudes at adjacent As atoms. This is consistent with the feature of PDOS's mentioned above. The interpolated band structure is then unfolded following the procedure of Ref. 21. The result is shown and compared with that for LaFeAsO in Figure 4. Here the width of the lines represents the weight of each Wannier function component. In the yz/zx panel, the weight is defined as the average of the weight of d_{yz} and that of

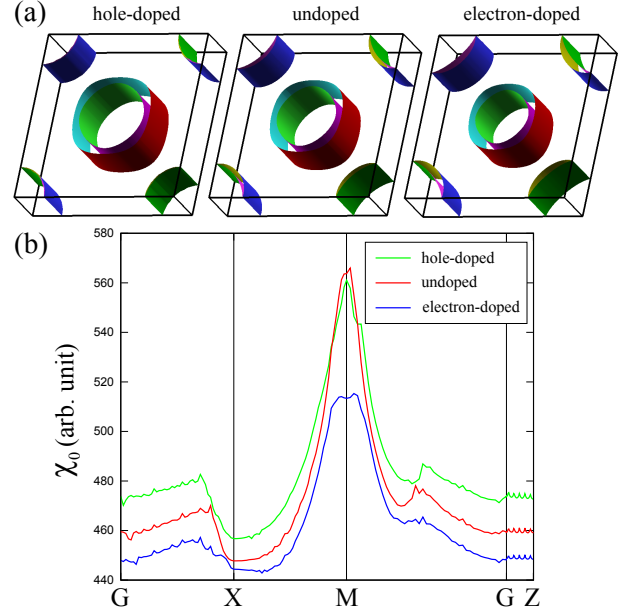


Fig. 3. (Color) (a) Fermi surfaces for hole-doped (left), undoped (middle) and electron-doped (right) $\text{Ca}_4\text{Al}_2\text{O}_6\text{Fe}_2\text{As}_2$, (b) Bare generalized susceptibility for these Fermi surfaces.

d_{zx} . Our convention for the x and y axes is the same as Fig.1 in Ref. 21. Namely, we define the x and y for the unit cell containing one Fe atom, whereas the X and Y refer to the original cell, which is rotated by 45 degrees from the x and y axes.

There are obvious differences in the band structure near $(0,0)$ and (π,π) points between the two com-

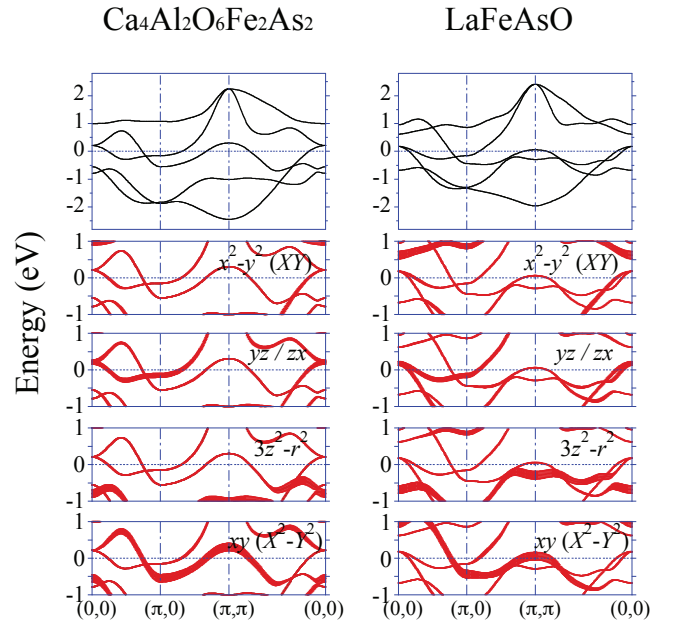


Fig. 4. (Color online) Unfolded band structure of $\text{Ca}_4\text{Al}_2\text{O}_6\text{Fe}_2\text{As}_2$ (left) and LaFeAsO (right). The width of the lines represent the weight of each maximally localized Wannier function. The Fermi level corresponds to the energy zero. The x and y refer to the unit cell containing one iron atom in the cell, whereas XY axis is rotated by 45 degrees, corresponding to the original cell.

pounds in Fig.4. In order to understand the origins of these differences, we calculated the band structure of $\text{Ca}_4\text{Al}_2\text{O}_6\text{Fe}_2\text{As}_2$ for different values of α while fixing both the Fe-As bond length and the distance between the As plane and the block layer. The band structure is shown in Fig.5, where the width of the lines represents the weight of the xy character. We can see that α does affect the band structure significantly. At $\alpha=105$ deg., a state appears at -0.3 eV at $(0,0)$. This is basically the case of $\text{Ca}_4\text{Al}_2\text{O}_6\text{Fe}_2\text{As}_2$ whose α is 102.13 degrees. As α increases, the state moves up and forms the hole-like Fermi surface in the case of $\alpha=110$ deg. With further increase of α , the band structure becomes similar to that of LaFeAsO whose α is 113.55 degrees. The behavior of the xy band near (π, π) with the change of α or the pnictogen height from the Fe plane is qualitatively the same as what was explained by Kuroki et al.¹⁰⁾ The xy band moves up above the Fermi level as α decreases and forms a hole pocket near (π, π) , whose presence may be a crucial condition for the strong superconductivity of $s\pm$ character. We also found that the distance between FeAs layer and block layer is another important parameter. With increasing the distance, the band rearrangement takes place at a larger value of α .

As suggested by the above arguments, the xy ($X^2 - Y^2$) orbital plays an important role in the band rearrangement. For the analysis of the behavior of this band, we list in Table I the onsite energy and the hopping integrals between xy ($X^2 - Y^2$) orbitals up to 5th neighbors, beyond which the hopping integrals are negligibly small. We note that the sign of t_1 and t_4 depends on the choice of the gauge. We take the opposite sign compared to Ref. 22. By cutting off the hopping integrals between different kinds of d orbitals, the band dispersion for the xy ($X^2 - Y^2$) orbitals is written as

$$\begin{aligned}
 E_{xy}(\mathbf{k}) = & \epsilon_{xy} + 2t_1[\cos(k_x) + \cos(k_y)] \\
 & + 4t_2 \cos(k_x) \cos(k_y) \\
 & + 2t_3[\cos(2k_x) + \cos(2k_y)] \\
 & + 4t_4[\cos(2k_x) \cos(k_y) + \cos(k_x) \cos(2k_y)]
 \end{aligned}$$

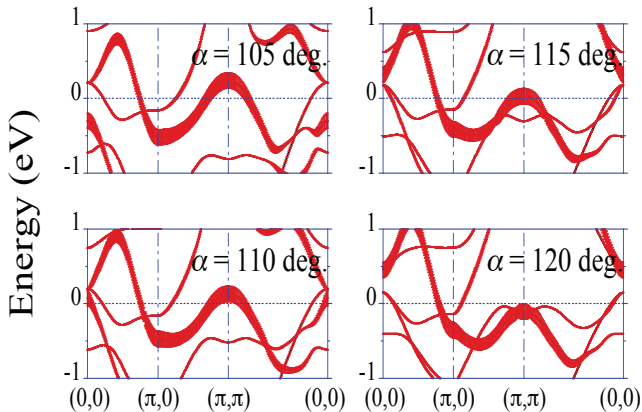


Fig. 5. (Color online) Unfolded band structure of $\text{Ca}_4\text{Al}_2\text{O}_6\text{Fe}_2\text{As}_2$ for the As-Fe-As angle $\alpha = 105, 110, 115$ and 120 degrees. The width of the lines represents the weight of the xy Wannier function. See the caption of Fig.4 for the convention of the xy axis.

$$+4t_5 \cos(2k_x) \cos(2k_y), \quad (1)$$

where ϵ_{xy} is the onsite energy, and t_n is the hopping integral for the n th neighbors. Now we can clearly understand why the xy band behaves quite differently between LaFeAsO and $\text{Ca}_4\text{Al}_2\text{O}_6\text{Fe}_2\text{As}_2$. First of all, the onsite energy of $\text{Ca}_4\text{Al}_2\text{O}_6\text{Fe}_2\text{As}_2$ is about 0.4 eV deeper than that of LaFeAsO (Table I and Fig.6) because of the change in the crystal field as implied by the difference in α . Secondly, the hopping integrals for the first three neighbors are quite different between the two compounds. Particularly the first neighbor hopping of $\text{Ca}_4\text{Al}_2\text{O}_6\text{Fe}_2\text{As}_2$ is very small in magnitude and has different sign from that of LaFeAsO. In Table I, the numbers in the parenthesis for t_1 denote the contributions from the direct d-d hopping. In the LaFeAsO case, the contribution from the indirect Fe-As-Fe hopping (0.394 eV) overwhelms the direct hopping (-0.243 eV) and the net hopping integral is 0.151 eV. However, in the $\text{Ca}_4\text{Al}_2\text{O}_6\text{Fe}_2\text{As}_2$ case, the indirect contribution (0.329 eV) and the direct contribution (-0.369 eV) nearly cancel each other to produce a small net hopping integral of -0.04 eV. The larger direct hopping for $\text{Ca}_4\text{Al}_2\text{O}_6\text{Fe}_2\text{As}_2$ is due to smaller Fe-Fe distance and the smaller indirect hopping is due to smaller α .

Using Eq. 1 and the parameters in Table I, we found that not only the difference in the onsite energy but also hopping integrals produce a large difference in the band energy at $(0,0)$ between the two compounds. In addition to this, the difference in the band energies between $(0,0)$ and (π, π) is $E_{xy}(\pi, \pi) - E_{xy}(0, 0) = -8(t_1 + 2t_4)$. Actual values for this quantity are -0.712 eV for LaFeAsO and $+0.848$ eV for $\text{Ca}_4\text{Al}_2\text{O}_6\text{Fe}_2\text{As}_2$. One may also notice in Fig.4 that the position of the $3z^2 - r^2$ branch near (π, π) is quite different between the compounds. For this aspect, we only mention that the trend in the onsite energy shown in Fig.6 is also enhanced by the hopping integrals as discussed for the xy ($X^2 - Y^2$) branch.

Now we discuss briefly other aspects of the band structure. As for the $x^2 - y^2$ (XY) and yz/zx states, the hopping integrals are qualitatively the same between LaFeAsO and $\text{Ca}_4\text{Al}_2\text{O}_6\text{Fe}_2\text{As}_2$. However, the variation in the onsite energies shown in Fig.6 may produce qualitatively important effects on the electronic structure of these states. In Fig.6, we first observe the splitting between the $d\epsilon(xy, yz, zx)$ states and the $d\gamma(x^2 - y^2, 3z^2 - r^2)$ states when the tetragonal distortion is small ($\alpha \sim 109.4$ deg.) in accordance with the ligand field theory for the tetrahedral symmetry. Further splitting among states within each of $d\epsilon$ and $d\gamma$ as α deviates from 109.4 deg. is a natural consequence of the distortion in the tetrahedral coordination. We also observe a quite interesting fact that the onsite energy of yz/zx states with respect to the Fermi level is nearly invariant for a wide range of materials with different α s. Other states particularly of $d\gamma$ become deeper and the energy separation from yz/zx states becomes larger as α decreases. This variation in the onsite energies leads to the increase of the weight of $d\epsilon$ states near the Fermi level as already pointed out by our previous papers.^{15,22)}

Finally we mention the strength of electron correla-

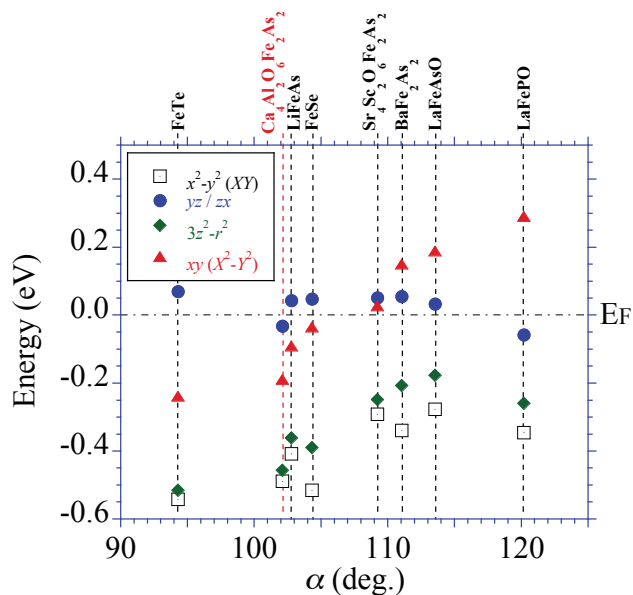


Fig. 6. (Color online) Onsite energy of each Wannier function for eight compounds as a function of the X -Fe- X angle, where X is the pnictogen / chalcogen atom. The Fermi level corresponds to the energy zero. See the caption of Fig.4 for the convention of the xy axis.

Table I. Orbital energy and hopping integrals up to fifth neighbors for xy ($X^2 - Y^2$) state (in eV). The notation with the X and Y axes is for easier comparison with the previous works on different compounds.^{22,25} See the caption of Fig.4 for the convention of X and Y axes. For t_1 , the numbers in parenthesis denote the contribution from the direct d-d hopping estimated by the dpp model.

	ϵ_{xy}	t_1	t_2
LaFeAsO	0.189	0.151 (-0.243)	0.117
Ca ₄ Al ₂ O ₆ Fe ₂ As ₂	-0.189	-0.040 (-0.369)	0.066
	t_3	t_4	t_5
LaFeAsO	-0.024	-0.031	-0.027
Ca ₄ Al ₂ O ₆ Fe ₂ As ₂	-0.012	-0.033	-0.029

tion. The onsite effective Coulomb interaction in the constraint random phase approximation (cRPA)^{23,24} are shown in Table II. The results of other iron-based superconductors using the same technique can be found in Ref. 22,25,26. The average of the diagonal terms is 3.08 eV, which is larger than that of LaFeAsO (2.53 eV) and substantially smaller than that of FeSe (4.24 eV).²² The exchange energy (not shown) is smaller than that of FeSe, and very close to that of LaFeAsO, with a slightly larger value for the xy orbital. The orbital anisotropy is weaker than LaFeAsO, reflecting that the xy ($X^2 - Y^2$) orbital is less extended.

In conclusion, we have studied the electronic structure of Ca₄Al₂O₆Fe₂As₂. We found that the topology of the Fermi surface is different from that of LaFeAsO. It is revealed that the As-Fe-As angle has strong impact on the band structure in the vicinity of the Fermi level around the (0,0) point, specifically through the change in the onsite energy level and transfer integral of the xy orbital.

Table II. Effective Coulomb interaction (U) on the same iron site for all the combinations of Wannier functions in units of eV. The definitions of X and Y axes are the same as those in Table I.

	XY	YZ	$3Z^2 - r^2$	ZX	$X^2 - Y^2$
XY	3.38	2.21	2.24	2.21	2.53
YZ	2.21	2.87	2.45	2.03	2.07
$3Z^2 - r^2$	2.24	2.45	3.46	2.45	2.11
ZX	2.21	2.03	2.45	2.87	2.07
$X^2 - Y^2$	2.53	2.07	2.11	2.07	2.82

It would be interesting to see how the pressure changes the properties of the compound. Relation with superconductivity is also an open question. Magnetic calculations including structural optimization are ongoing and will be published elsewhere.

The authors are grateful to Dr. P. M. Shirage, Dr. K. Kihou, Dr. C.-H. Lee, Dr. H. Kito, Dr. H. Eisaki and Dr. A. Iyo for providing us with experimental data prior to publication. The authors also acknowledge Prof. K. Kuroki for discussions. The present work is partially supported by the Next Generation Supercomputer Project, Nanoscience Program, and by a Grant-in-Aid for Scientific Research on Innovative Areas under grant No. 22104010 from MEXT, Japan.

- 1) Y. Kamihara, T. Watanabe, M. Hirano and H. Hosono: J. Am. Chem. Soc. **130** (2008) 3296.
- 2) M. Rotter, M. Tegel, D. Johrendt, I. Schellenberg, W. Hermes and R. Pöttgen: Phys. Rev. B **78** (2008) 020503(R).
- 3) J.H. Tapp, Z. Tang, B. Lv, K. Sasmal, B. Lorenz, P. C. W. Chu, and A. M. Guloy: Phys. Rev. B **78** (2008) 060505(R).
- 4) Y. Shimizu, H. Ogino, N. Kawaguchi, K. Kishio and J. Shimoyama: arXiv:1006.3769 and references therein.
- 5) H. Ogino, K. Machida, A. Yamamoto, K. Kishio, J. Shimoyama, T. Tohei and Y. Ikuhara: arXiv:1008.2582.
- 6) P.M. Shirage, K. Kihou, C.-H. Lee, H. Kito, H. Eisaki and A. Iyo: arXiv:1008:2586.
- 7) C.-H. Lee, A. Iyo, H. Eisaki, H. Kito, M. T. Fernandez-Diaz, T. Ito, K. Kihou, H. Matsuhata, M. Braden, and K. Yamada: J. Phys. Soc. Jpn. **77** (2008) 083704.
- 8) J. Zhao, Q. Huang, C. d. l. Cruz, S. Li, J. W. Lynn, Y. Chen, M. A. Green, G. F. Chen, G. Li, Z. Li, J. L. Luo, N. L. Wang and P. Dai: Nature Materials **7** (2008) 953.
- 9) V. Vildosola, L. Pourovskii, R. Arita, S. Biermann, and A. Georges: Phys. Rev. B **78** (2008) 064518.
- 10) K. Kuroki, H. Usui, S. Onari, R. Arita, and H. Aoki: Phys. Rev. B **79** (2009) 224511.
- 11) <http://qmas.jp>
- 12) P.E. Blöchl: Phys. Rev. B **50** (1994) 17953.
- 13) S. Ishibashi, K. Terakura and H. Hosono: J. Phys. Soc. Jpn. **77** (2008) 053709.
- 14) S. Ishibashi and K. Terakura: J. Phys. Soc. Jpn. **77** (2008) Suppl. C, pp. 91.
- 15) S. Ishibashi and K. Terakura: Physica C (2009), doi:10.1016/j.physc.2009.11.035.
- 16) J.P. Perdew, K. Burke and M. Ernzerhof: Phys. Rev. Lett. **77** (1996) 3865.
- 17) N. Marzari and D. Vanderbilt: Phys. Rev. B **56** (1997) 12847.
- 18) I. Souza, N. Marzari, and D. Vanderbilt: Phys. Rev. B **65** (2001) 035109.
- 19) M. Methfessel, M. van Schilfhaarde, and R. A. Casali, in Lecture Notes in Physics, edited by H. Dreyse (Springer-Verlag, Berlin, 2000), Vol. 535.
- 20) S.H. Vosko, L. Wilk, and M. Nusair, Can.J.Phys. **58** (1980) 1200.

- 21) K. Kuroki, S. Onari, R. Arita, H. Usui, Y. Tanaka, H. Kontani and H. Aoki: Phys. Rev. Lett. **101** (2008) 087004.
- 22) T. Miyake, K. Nakamura, R. Arita, and M. Imada: J. Phys. Soc. Jpn. **79** (2010) 044705.
- 23) F. Aryasetiawan, M. Imada, A. Georges, G. Kotliar, S. Biermann and A.I. Lichtenstein, Phys. Rev. B **70**, (2004) 195104.
- 24) T. Miyake and F. Aryasetiawan: Phys. Rev. B **77** (2008) 085122; T. Miyake, F. Aryasetiawan and M. Imada: Phys. Rev. B **80** (2009) 155134.
- 25) K. Nakamura, R. Arita and M. Imada: J. Phys. Soc. Jpn. **77** (2008) 093711.
- 26) T. Miyake, L. Pourovskii, V. Vildosola, S. Biermann, and A. Georges: J. Phys. Soc. Jpn. **77** (2008) Suppl. C, 99.